THE JOURNAL OF PHYSICAL CHEMISTRY C
A JOURNAL OF THE AMERICAN CHEMICAL SOCIETY

pubs.acs.org/JPCC

Article

Anisotropy of Shear-Induced Mechanochemical Reaction Rates of Surface Adsorbates; Implications for Theoretical Models

Resham Rana, Germaine Djuidje Kenmoe, François Sidoroff, Robert Bavisotto, Nicholas Hopper, and Wilfred T. Tysoe*

Cite This: *J. Phys. Chem. C* 2022, 126, 11585–11593

Read Online

ACCESS | Metrics & More | Article Recommendations | Supporting Information

ABSTRACT: Mechanochemical reactions occur by an applied force modifying and ideally accelerating the rate of reaction of a mechanically active species, a mechanophore. Thermal reactions are described by the steepest descent pathway (SDP) of the potential energy surface (PES) from the transition state to the reactant state, which are stationary points on the SDP. The activation energy is calculated from the energy difference between these two points. The PES is modified by an imposed force to yield a reaction pathway given by the force-displaced stationary points (FDSPs), which depend on the magnitude and direction of the force and shape of the PES. However, the SDP has zero force in a direction perpendicular to it so that the PES can be visualized as a "harmonic valley" that forms a potential energy trough about the SDP. If the walls of the potential trough are sufficiently steep, a mechanochemical reaction should be constrained to occur along the SDP, and the influence of an applied force should depend only on the component of the force along it. If this is the case, it should be possible to use just the shape of the PES around the initial and transition states to calculate the effect of an imposed force or stress on mechanochemical reaction rates. The postulate is tested for the mechanically induced decomposition of an adsorbed methyl thiolate species on a Cu(100) single-crystal surface by measuring the azimuthal angular dependence of the mechanochemical methyl thiolate decomposition rate by varying the sliding direction of a sharp atomic force microscope tip over the surface in ultrahigh vacuum. The concept is also illustrated using a model 4-fold potential using a Remoissenet–Peyrard function to mimic the potential of a Cu(100) surface. This yields an angular dependence that agrees well with the prediction from the above postulate. This simplification will facilitate the analysis of mechanochemical rates of both surface and bulk reactions.

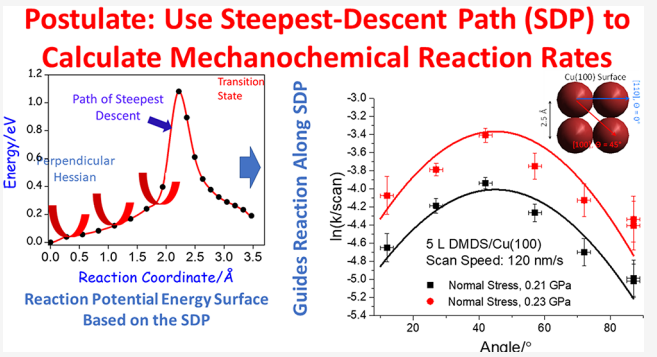

INTRODUCTION

Of the four ways in which chemical reaction rates can be accelerated, by heat, by photons, by electrons, or by force, the latter, which constitutes the subfield of mechanochemistry, is arguably the least well understood. Insights into mechanisms of mechanochemical reaction kinetics have come from sensitive single-molecule pulling experiments[1,2] in which forces are exerted at a specific pulling point (PP) relative to an attachment point (AP) to distort the mechanophore and to influence the rates and selectivities of chemical reactions. Very large forces ultimately result in bond scission, and there has recently been significant activity in the area of molecular mechanochemistry.

An advantage of such single-molecule systems is that they facilitate the modeling of the coupling between the force and reactivity because the force is applied to well-defined attachment points on the mechanophore. One of the first theoretical approaches, the constrained geometries simulate external force (CoGEF)[3] method, displaces the AP and PP and then allows the perturbed system to relax to a new stable configuration to calculate the energy as a function of the force. The accuracy of this approach has recently been validated,[4] and the correct reaction pathway is automatically obtained during the structural optimization step. Other approaches include both the force-modified potential energy surface (FMPES) method,[5,6] in which the Born–Oppenheimer potential energy surface (PES) is modified by directly including the effect of the forces on the AP and PP, and the analogous EFEI (external force is explicitly included) method.[7]

In most cases, the results show that the activation energy decreases from its value in the absence of a force, E_{act}. For low forces, it varies as $E_{act}(F) = E_{act} + F\Delta x^{\ddagger}$, where F is the force exerted at the pulling point(s) and $\Delta x^{\ddagger}$ is an activation length

Received: May 2, 2022
Revised: June 27, 2022
Published: July 7, 2022

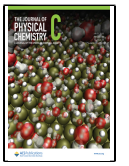

Scheme 1. Mechanochemical Reaction Pathway of Methyl Thiolate Species on Cu(100), Where k_1 and k_2 Are the Reaction Rate Constants for Each Process

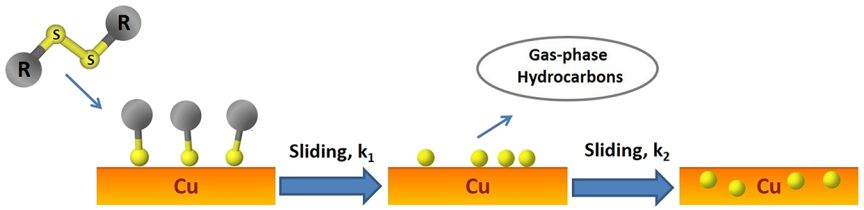

defined as the distance between the PP and AP in the reactant and transition states[8] and negative values causes the reaction rate to increase with force. This is often known as the Bell equation and was originally applied to analyzing cell adhesion.[9] More accurate formulae have been proposed that include the effect of the compliances of the initial and transition states[10,11] that result in an F^2 dependence.[12]

It is worth noting that similar concepts have been used to model mechanically induced energy dissipation processes where, in contrast to mechanochemistry, the transition over the energy barrier preserves the state of the system and only dissipates energy;[13] friction is analyzed using the Prandtl−Tomlinson model[14] and Eyring used similar ideas to model liquid viscosity.[15] The model by Prandtl also found a nonlinear force dependence of the activation barrier from an analysis of the energy as it approached a critical force F^* when the energy barrier reduces to zero as $E(F)\sim(F^* - F)^{3/2}$. Several reviews discuss these concepts in greater detail.[16]

While single-molecule pulling provides model systems that are amenable to fundamental analysis, this is generally not the way in which mechanochemical reactions are carried out in practice. Perhaps the oldest approach to measuring mechanochemical reaction rates was to use hydrostatic pressure[17] or by using sonochemistry[18] for both fundamental studies and as a synthetic tool.[19] As a result, the first analysis of mechanochemical reaction rates was by Evans and Polanyi based on transition-state theory[20] to yield an equation for the hydrostatic-pressure-dependent rate constant k: $\partial \frac{\ln k}{\partial P}\Big|_T = -\frac{\Delta V^{\ddagger}}{RT}$, where P is the pressure, R is the gas constant, and T is the absolute temperature. $\Delta V^{\ddagger}$ is known as an activation volume and broadly corresponds to a volume difference between the initial and transition-state structures. If the rate constant in the absence of a pressure is k_0, integration yields $k(P) = k_0 \exp\left(-\frac{P\Delta V^{\ddagger}}{RT}\right)$ so that the Bell equation becomes $E_{act}(P) = E_{act} + P\Delta V^{\ddagger}$ and the reaction rate increases exponentially with pressure for negative activation volumes in a way that depends on $\Delta V^{\ddagger}$. As a result, Stearn and Eyring suggested that the activation volume is equal to $A\Delta x^{\ddagger}$,[21] where A represents an area over which the stresses act. The rates of pressure-induced reactions have been calculated by enclosing the reactant(s) in a van der Waals' cocoon and by computing the reaction activation energy as a function of the size of the cocoon to vary the pressure and to thereby calculate activation volumes in an FMPES-type approach.[6,22]

In practice, however, mechanochemical reactions are often carried out using a ball mill.[1,8,12,23,24] Because they do not require solvents, they are more environmentally friendly than conventional organic syntheses.[24] Perhaps, the most economically important mechanochemical processes are those occurring at sliding contacts interfaces in machines[25,26] with high interfacial pressures in the GPa range.[27]

In these cases, mechanochemical reactions are induced at a solid−solid contact. Understanding such processes has their own unique challenges compared to the pulling experiments described above. The first is to identify the surface mechanochemical reaction pathway. This has been accomplished for simple mechano-active adsorbates in ultrahigh vacuum (UHV).[28] For example, the mechano/tribochemical reaction pathways of methyl thiolate species on copper have been extensively investigated[29−32] and been found to proceed by the adsorbed methyl thiolate species tilting toward the surface to induce C−S bond scission to evolve small gas-phase hydrocarbons and deposit sulfur on the surface.[30,32,33] This is followed by a process in which shear causes the sulfur to be driven into the subsurface region to regenerate a clean surface,[34] as illustrated in Scheme 1, where k_1 and k_2 are the rate constant for the mechanochemical reaction steps and they have been measured. The methyl thiolate tilting that occurs as the reaction proceeds is intuitively expected to cause the reaction to accelerate by the imposition of both normal and lateral forces, and the increase in reaction rate found by just a normal stress agrees with this idea.[26]

In the following, the mechanochemical reaction rate is measured experimentally by sliding an atomic force microscope (AFM) tip over a methyl-thiolate-covered Cu(100) single crystal in UHV to induce tribochemical reactions. This approach has several advantages. First, the stresses can be calculated for an elastic, nanoscale, ball-on-flat geometry.[35] Second, the area over which the stress acts is easily calculated from the coverage to enable an activation volume to be calculated from the activation length.

However, such results cannot easily be analyzed using the mechanochemical reaction theories described above because there is no clearly identifiable PP and AP. A central assumption that underpins the models of mechanochemical reaction rates is that the potential energy surface (PES), $V(\underline{r})$, for the reaction, is modified by a potential, $\int \underline{F}\cdot d\underline{r}$, due to an imposed mechanical force, $\underline{F}$, to change the energies and positions of the reactant and transition states to alter, and generally accelerate, the reaction rate.[6,22] Note that the transitions over the modified barrier are still thermally driven. The force-modified potential energy surface (FMPES), $V(\underline{r}, \underline{F})$, is given as

$$V(\underline{r}, \underline{r}) = V(\underline{r}) - \int \underline{F}\cdot d\underline{r} \tag{1}$$

where $\underline{r}$ is the position vector of the atoms in the system. The effect of the force on the initial- and transition-state energies is given by the stationary points of eq 1[36] to yield

$$\frac{\partial V(\underline{r}, \underline{F})}{\partial \underline{r}} = \underline{\nabla}_r V(\underline{r}) - \underline{F} = 0 \tag{2}$$

https://doi.org/10.1021/acs.jpcc.2c03033
J. Phys. Chem. C 2022, 126, 11585−11593

Accordingly, the value of $\delta \underline{r}$, a displacement on the modified PES that is induced by a change in force, $\delta \underline{F}$, is given by

$$\frac{\delta \underline{F}}{\delta \underline{r}} \approx \frac{d\underline{F}}{d\underline{r}} = \underline{\nabla}_r^2 V(\underline{r}) = \underline{H} \tag{3}$$

where $\underline{H}$ is the Hessian matrix evaluated on the PES to give

$$\delta \underline{r} = \underline{H}^{-1} \delta \underline{F} \tag{4}$$

to define the effect of an imposed force on an arbitrary PES. Thus, the mechanochemical reaction path is described by the force-displaced stationary points (FDSPs) emanating from the reactant and transition states that evolve as the force increases to cause a reduction in the energy barrier. These points eventually coalesce to form a singularity at a force F^* that reduces the energy barrier to zero.

The CoGEF, FMPES, and EFEI methods automatically guide the reaction along the FDSPs, which depend on the direction of the force relative to the mechanophore. For example, the surface mechanochemical decomposition of acetate mechanophores on copper depends on the sliding direction relative to the mirror plane formed by the adsorbed carboxylate group.[37]

In the case of a chemical reaction, the general topology of the PES is reasonably well understood.[38] The structural evolution of the reaction is given by the steepest descent pathway (SDP), s, the arc length along the reaction path from the transition state, which is a saddle point in the PES, to the reactant, which is a local minimum. The PES perpendicular to s is, by definition, a local minimum and thus has a positive curvature given by a projected force constant matrix, $\boldsymbol{K}(s)$.[39] As a result, the region of the PES that is relevant to chemical reactions can then be thought of as consisting of a "harmonic valley" that forms a potential energy trough about the reaction path. If the elements of $\boldsymbol{K}(s)$ are sufficiently large, the mechanochemical reaction will be guided along the SDP and thus depend only on the component of the imposed force along it. If this were the case, it would significantly facilitate the analysis of mechanochemical reaction kinetics because it would allow the effect of an applied stress to be calculated just for the reactant and transition-state structures, which can be obtained using approaches such as the nudged elastic band (NEB) method.[38]

This idea is tested here by measuring the mechanochemical reaction rate for the decomposition of methyl thiolates adsorbed on a well-ordered Cu(100) single crystal (Scheme 1) as a function of sliding direction. If the postulate is correct, the mechanochemical rate will depend just on the component of the force along the SDP. Note that anisotropies in friction forces have been measured, often for small crystallites sliding against a crystalline substrate. The best-known example is for a small graphene flake sliding over a crystalline graphite substrate, where large anisotropies are found associated with the difference in registry between the lattices of the contacting materials as a function of their relative orientations.[40] The postulate is illustrated using a model analytical function to represent a 4-fold PES that allows the FDSPs to be obtained to calculate the activation length as a function of the direction of the force.

EXPERIMENTAL METHODS

Experiments were carried out using an RHK variable-temperature ultrahigh-vacuum (UHV) AFM operating at a base pressure of $\sim 2 \times 10^{-10}$ Torr following bakeout, as described previously.[26] The apparatus also contained an analysis chamber for sample cleaning and was equipped with a Scienta Omicron SPECTALEED combined low-energy electron diffraction (LEED)/Auger electron spectroscopy system for assessing sample cleanliness, crystalline order, and the orientation of the Cu(100) single crystal relative to the AFM sliding direction. The experimental angles were measured relative to the [110] directions of the Cu(100) crystal by determining its orientation using LEED. This was related to the sliding direction of the "beetle" head using a clean Au(111) single crystal, where the scanning orientation relative to the substrate lattice could be measured from the clearly visible "herringbone" reconstruction seen in the scanning tunneling microscopy (STM) image.[41]

Reaction rates were measured by reciprocating sliding of a silicon μ-masch (HQ:NSC19/NO AL) AFM tip with a nominal 8 nm radius as a function of sliding direction using a speed of 120 nm/s over a length of 60 nm at applied loads of 30 and 40 nN. The loads were corrected for adhesion force.[42] The rates were obtained from the depths of the wear tracks, which were taken to be proportional to the extent of reaction, measured using AFM at low, nonperturbative loads as a function of the number of scans across the surface. The reacted region remained stable for a sufficient time to measure its topography.[26] The depths d were found to vary exponentially with the number of scans s as $d = d_0(1 - \exp(-ks))$, where d_0 is the final depth of the wear track and k is the corresponding first-order rate constant. The error bars in the experimental data reflect the noise in the images used to measure the depths. Note that the lateral forces could not be measured for different sliding directions because the AFM cantilever tilt could not be monitored at all angles. The chamber was also equipped with a Dycor quadrupole mass analyzer for leak checking and background gas analysis.

The Cu(100) single crystal was cleaned by argon ion bombardment ($\sim$1 kV, $\sim 2\ \mu A/cm^2$) and then by annealing to $\sim$850 K to remove any surface damage induced by the cleaning procedure. Saturated methyl thiolate overlayers were prepared by background dosing a clean Cu(100) sample held at $\sim$298 K in UHV with dimethyl disulfide (DMDS, Aldrich, 99.0% purity) at a pressure of 1×10^{-8} Torr for 500 s, where the pressures were measured using a nude ionization gauge included in the UHV chamber. The pressures were not corrected for ionization gauge sensitivity.[43] The DMDS was transferred to a glass bottle and attached to the gas-handling system of the vacuum chamber and cleaned by several freeze-pump-thaw cycles. The purity was monitored using mass spectroscopy. Sulfur-containing regions on the Cu(100) surface were prepared by decomposing a methyl thiolate overlayer on Cu(100) by heating to $\sim$415 K at a rate of 4.3 K/s.[43]

The cantilever force constant was calculated from its dimensions measured by scanning electron microscopy (SEM) as described in ref 44 and by the Sader method.[45] SEM was also used to verify the integrity of the AFM tip after performing the experiments. Force−distance curves measured periodically between experiments verified that the tip shape had not changed after conditioning. The tips were found to remain stable over multiple sliding experiments, but the maximum experimental pressure was limited to minimize the chance of tip failure. The normal stresses were obtained by

https://doi.org/10.1021/acs.jpcc.2c03033
J. Phys. Chem. C 2022, 126, 11585−11593

using the width of the wear track to estimate the contact area.[26]

RESULTS

Experiments were carried out by repeatedly rubbing a saturated methyl thiolate overlayer on a Cu(100) single-crystal substrate as a function of the sliding direction to create grooves in the overlayer that could be imaged at a lower, nonperturbative load to allow the depth of the groove to be measured as a function of the number of scans. Figures S1 and S2 of the Supplementary Information section illustrate that the mechanochemically formed products in the AFM are identical to those formed in the UHV tribometer (Scheme 1). Images of the rubbed regions are shown in Figure S3 of the Supplementary Information section, and a typical plot of the depth of the groove as a function of the number of scans is shown in Figure 1.

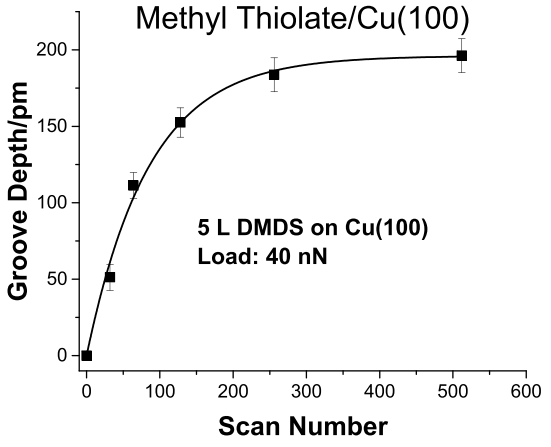

Figure 1. Plot of the depth of the groove caused by rubbing a methyl-thiolate-covered Cu(100) sample using an AFM tip at an applied load of 40 nN, corresponding to a normal stress of 0.23 GPa, as a function of the number of scans, indicated as scan number. The line is an exponential fit to the data to yield a maximum groove depth d_0= 196 ± 8 pm, consistent with the thickness of a methyl thiolate overlayer on Cu(100). This yields a first-order reaction with a rate constant of 0.012 ± 0.001 scan^{-1}.

The results fit well to an exponential growth rate and indicate that the mechanochemical removal of methyl thiolate occurs with first-order kinetics, as found previously.[30,46] Based on these results, the depths of the grooves were measured as a function of scan angle after rubbing 256 times at a normal load of 30 nN and for 64 scans at 40 nN to obtain the first-order reaction rate constants per scan, k/scan. The widths of the tracks formed during each experiment were used to estimate the contact areas for each load and indicated that the average contact stress was 0.21 GPa for a 30 nN load and 0.23 GPa for a load of 40 nN. This is in the same range as the contact pressures in the ball-on-flat geometry in the UHV tribometer, estimated to be between 0.1 and 0.4 GPa depending on the choice of the contact model.[31]

The results for the angular-dependent reaction rates at two different normal stresses are displayed in Figure 2, plotted as ln(k/scan) versus the scan angle relative to the [110] directions. The data show an angular dependence, with a maximum at a value of the rate constant at a scan angle of 45°. The rates are identical for both positive and negative deviations from the [110] directions, as expected from the

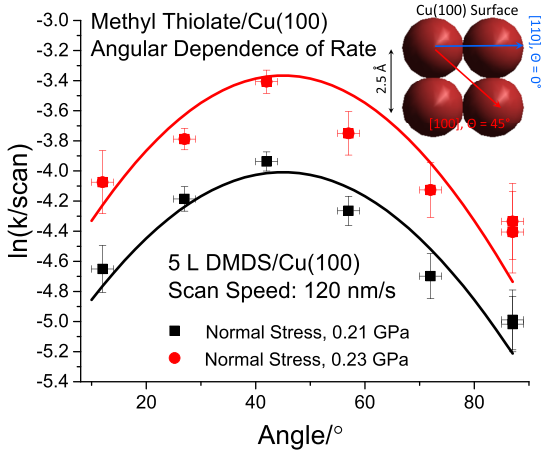

Figure 2. Plot of $\ln\left(\frac{k}{\text{scan}}\right)$, where k is the rate constant for the shear-induced decomposition of methyl thiolate species on Cu(100), as a function of scanning angle relative to the [110] directions, illustrated as an inset to the figure. Experiments were carried out at normal stresses of 0.21 GPa (solid black box) and 0.23 GPa (solid red box). The solid lines plotted with the data are fits assuming that $\ln(k_0)\approx -8.7$.

symmetry of the substrate. The solid lines through the data represent fits to theory as discussed below.

DISCUSSION

Methyl thiolate species on copper have been previously found to undergo shear-induced (tribochemical) decomposition on copper to desorb small gas-phase hydrocarbons and deposit sulfur on the surface in a first-order process (Scheme 1),[30,46] consistent with the measured kinetics (Figure 1) and reaction products (Figures S1 and S2). Nudged-elastic band (NEB) calculations of the reaction pathway on Cu(100) show that it reacts by an initially vertical thiolate species tilting along the [100] directions on the surface to initiate C−S bond scission.[31]

The energies and structures of the initial and transition states and the steepest descent pathways for surface reactions can be quite accurately obtained using DFT[38] so that it would be advantageous if mechanochemical reactions could be analyzed using the SDP. We postulate that sufficiently large values of $\boldsymbol{K}(s)$, where s is the arc length along the SDP, should constrain the reaction to remain on the SDP. The calculated values of $\boldsymbol{K}(s)$ for thiolate decomposition on Cu(100) are plotted in Figure 3. In the initial state, the force constants are identical along directions parallel and perpendicular to the SDP because of symmetry, at a value of ∼0.75 N/m. This value remains reasonably constant as the reaction proceeds. The translational force constant is even larger (∼35 N/m) and suggests that the reaction should be constrained to remain on the SDP.

To further illustrate these ideas, the FDSPs were calculated numerically using a model 4-fold modified Remoissenet−Peyrard (R−P) function[47] to mimic the PES of the 4-fold Cu(100) surface

$$V(x,y)=\frac{E_{\text{act}}(1+r^2)(1-\cos(\pi x/a)\cos(\pi y/a))}{(1+r^2+2r\cos(\pi x/a)\cos(\pi y/a))} \quad (5)$$

where a is the periodicity of the lattice and r is a parameter such that $|r| < 1$. This influences the shape of the potential (not to be confused with the position vector $\underline{r}$) and, in particular, its

https://doi.org/10.1021/acs.jpcc.2c03033
J. Phys. Chem. C 2022, 126, 11585−11593

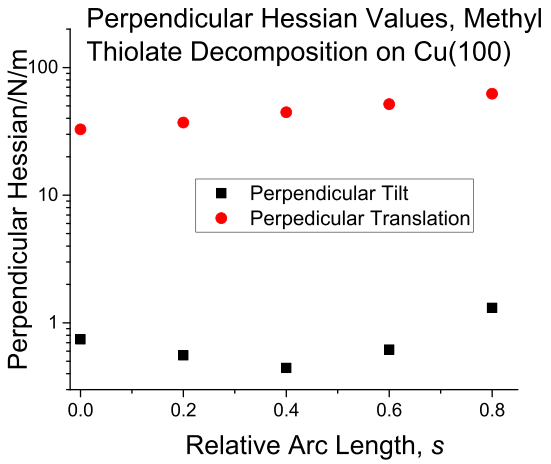

Figure 3. Plot of the force constants perpendicular to the steepest descent path, $\boldsymbol{K}(s)$, where s is the arc length along the reaction pathway for the decomposition of methyl thiolate species on Cu(100) for (black solid box) perpendicular tilts of the methyl thiolate species and (red solid circle) translations perpendicular to the steepest descent path.

steepness perpendicular to the SDP. When $r = 1$, this yields a two-dimensional sine function as shown in Figure 4. The

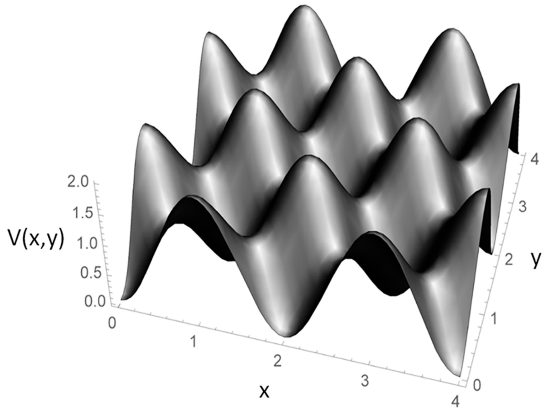

Figure 4. Two-dimensional depiction of the modified R−P potential, $V(x, y)$, with $r = 0$ used for modeling the PES for mechanochemical reactions on Cu(100).

function has periodic global minima at $x = y = 0$, where $\cos(\pi x/a) = \cos(\pi y/a) = 1$, which, when substituted into eq 5, gives $V(0,0) = E_{min} = 0$. A saddle point occurs at $x = y = \frac{a}{2\pi}$. This yields $\cos(\pi x/a) = \cos(\pi y/a) = 0$, and substitution into eq 5 gives $V\left(\frac{a}{2\pi}, \frac{a}{2\pi}\right) = E_{act}$, the energy at the saddle point. Thus, the SDP follows a line defined by $x = y$ and gives an activation length $\Delta x^{\ddagger} = \frac{a}{\sqrt{2}}$. A global maxima in the potential occur at $x = 0$, $y = a$ to give $\cos(\pi x/a) = 1$, $\cos(\pi y/a) = -1$ and yields

$$E_{max} = 2E_{act}\frac{1 + r^2}{(1 - r)^2} \tag{6}$$

The effect of r on the PES is shown in Figure 5 and emphasizes that the activation energy is independent of r. The maximum in the potential occurs along a line defined by $x + y = 1$ (Figure 5b), and the SDP occurs along a trajectory that passes through the saddle point along $x = y$ so that the activation energy is independent of r. The value of r for any particular value of E_{max}/E_{act} can be calculated from $r = \frac{\left(\frac{E_{max}}{E_{act}}\right) - 2\sqrt{\left(\frac{E_{max}}{E_{act}}\right) - 1}}{\left(\frac{E_{max}}{E_{act}}\right) - 2}$.

The FDSPs emanating from the initial and transition states are calculated for different values of r of the R−P function for forces along different directions, and the resulting force-dependent energy barriers are shown in Figure 6 as a function of force for various values of r. The plots show nonlinear behavior, where the slopes of the initial, linear region are equal to $\Delta x^{\ddagger}$ in the Bell equation, while the curvatures of the plots illustrate the nonlinear effects.[11] The forces at which the energy barrier decreases to zero is F^*. However, experimentally accessible stresses generally only cause modest decreases in the activation energy,[26] so the results are plotted showing only the initial decrease in Figure 7 (left panel).

This reveals that the lines with various values of r, which are colored in black, red, and green, overlap each other and show essentially identical variations in activation energy with applied force. This is consistent with the postulate that the FDSP coincides with the SDP. The variation in activation length, $\Delta x^{\ddagger}$, is shown in Figure 7 (right panel), where the line through the data illustrates the cosine dependence.

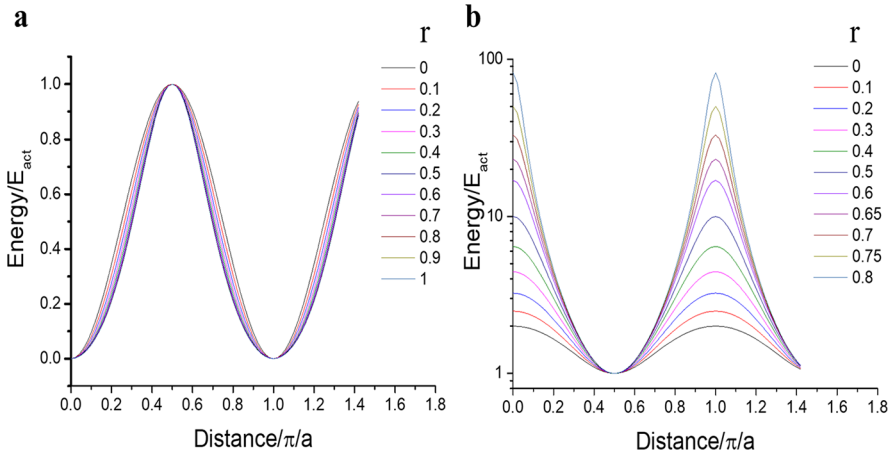

Figure 5. Energy profiles (a) along $x = y$ (the minimum-energy pathway) and (b) along $x + y = 1$ (across a maximum), as a function of r.

https://doi.org/10.1021/acs.jpcc.2c03033
J. Phys. Chem. C 2022, 126, 11585−11593

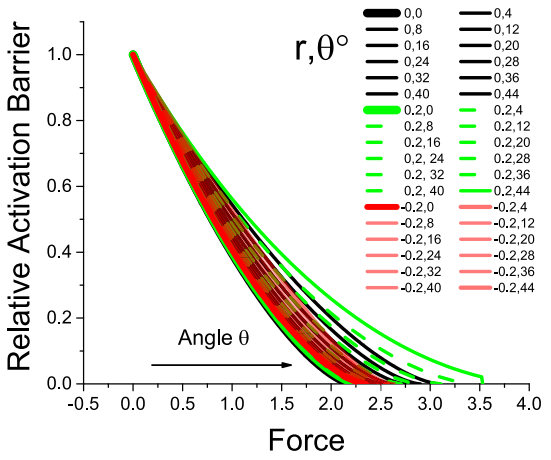

Figure 6. Theoretical results of the relative activation barrier as a function of force until the barrier vanishes for different values of r and azimuthal angles of the applied force.

Thus, the postulate predicts that sliding at an angle θ to the SDP (along the [100] directions) should cause the rate to change according to the component of the force along this direction. However, there are four symmetrically equivalent directions on the (100) surface, so that, as the sliding angle changes, the force has component along the orthogonal direction, that varies as sin θ. The total rate is the sum of both contributions to give an overall cos θ + sin θ dependence, where the maximum rate will be for sliding at 45° to the [100] direction. This is in agreement with the data shown in Figure 2.

The solutions obtained by using the R−P potential in Figure 7 predict that the azimuthal stress-dependent activation energy is given by $E_{act}(F) = E_{act} + \sigma(\cos\theta + \sin\theta)\Delta V^{\ddagger}$, where σ is an applied stress. Since the rate constant depends exponentially on the activation energy, this equation can be written in terms of the rate constants as $\ln(k(\sigma)) = \ln(k_0) + \frac{\sigma\Delta V^{\ddagger}}{k_B T}(\cos\theta + \sin\theta)$, where $k_0 = A\exp\left(-\frac{E_{act}}{RT}\right)$. This equation is shown fitted to the experimental results in Figure 2 (solid lines), where the agreement between theory and experiments is reasonable. The two sets of data were fit using an identical value of $\ln(k_0) \approx -8.7$, where the rate constants are measured in units of the time for the tip to pass over a point on the surface. Both fits also used the same value of $\frac{\Delta V^{\ddagger}}{k_B T} \approx -16.2 \pm 0.2$, indicating that the activation energy does scale linearly with the applied stress.

These results confirm that the idea suggested above that the force-displaced stationary points (FDSP) on the potential energy surface that describe the mechanochemical reaction coincide with the path of steepest descent when the values of $\boldsymbol{K}(s)$ are sufficiently large. This indicates that the influence of forces/stresses on the activation energy can be calculated from the effect on just the initial- and transition-state structures obtained for the minimum-energy pathway. This will not only significantly simplify the calculation of mechanochemical reaction rates but also will provide insights into which parameters most strongly influence the mechanochemical reactivity.

CONCLUSIONS

Angular-dependent AFM sliding experiments on a methyl thiolate overlayer on a well-ordered Cu(100) single-crystal substrate have been carried out to measure the mechanochemical reaction rates of methyl thiolate decomposition as a function of sliding direction to test the postulate that the path of steepest descent can be used to describe the effect of stresses on the rates of mechanochemical reactions. This predicts that the reaction rate should depend on the component of the applied stress lying along the SDP, and this is found experimentally to be the case. This insight will significantly facilitate the analysis of stress-induced mechano- and tribological reactions because the stress-dependent activation energy can be calculated from the effect of an applied stress on the initial- and transition-state structures, which can be obtained in a straightforward way using well-developed strategies. This insight will enable the effects that influence mechanochemical reaction rates for adsorbates on surfaces and in the bulk to be understood to be able to eventually design either mechano-active or mechano-resistant materials.

Finally, knowing how the rate of the tribochemical decomposition of methyl thiolate depends on the sliding direction will enable precise and reliable measurements of the stress-dependence of the rates to be made to understand how normal and shear stress couple to accelerate the rates of chemical reactions.

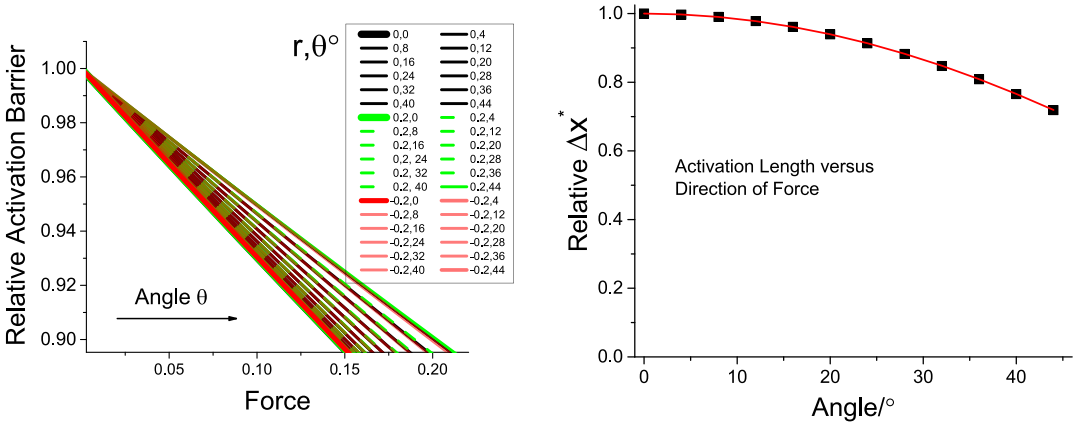

Figure 7. (Left panel) Close up view of theoretical results of the relative activation barrier as a function of force until the barrier is reduced to ∼10% of initial value, for different values of r and azimuthal angle of the applied force. (Right panel) Relative change in the activation length as a function of azimuthal angle of the applied force.

https://doi.org/10.1021/acs.jpcc.2c03033
J. Phys. Chem. C 2022, 126, 11585−11593

■ ASSOCIATED CONTENT

Supporting Information

The Supporting Information is available free of charge at https://pubs.acs.org/doi/10.1021/acs.jpcc.2c03033.

Figures S1 to S3 and a description of the analysis of the surface after rubbing (PDF)

■ AUTHOR INFORMATION

Corresponding Author

Wilfred T. Tysoe − *Department of Chemistry and Biochemistry, University of Wisconsin-Milwaukee, Milwaukee, Wisconsin 53211, United States;* orcid.org/0000-0002-9295-448X; Email: wtt@uwm.edu

Authors

Resham Rana − *Department of Chemistry and Biochemistry, University of Wisconsin-Milwaukee, Milwaukee, Wisconsin 53211, United States*

Germaine Djuidje Kenmoe − *Department of Chemistry and Biochemistry, University of Wisconsin-Milwaukee, Milwaukee, Wisconsin 53211, United States; Laboratory of Mechanics, Faculty of Science, University of Yaounde I, Yaounde, Cameroon*

François Sidoroff − *Laboratoire de Tribologie et Dynamique des Systèmes, CNRS UMR5513, Ecole Centrale de Lyon, Ecully F-69134, France*

Robert Bavisotto − *Department of Chemistry and Biochemistry, University of Wisconsin-Milwaukee, Milwaukee, Wisconsin 53211, United States*

Nicholas Hopper − *Department of Chemistry and Biochemistry, University of Wisconsin-Milwaukee, Milwaukee, Wisconsin 53211, United States*

Complete contact information is available at: https://pubs.acs.org/10.1021/acs.jpcc.2c03033

Notes

The authors declare no competing financial interest.

■ ACKNOWLEDGMENTS

We gratefully acknowledge the Civil, Mechanical, and Manufacturing Innovation (CMMI) Division of the National Science Foundation under grant number 2020525 for support of this work. W.T.T. thanks LABEX Manutech-Sise (ANR-10-LABX-0075) of Université de Lyon, within the program "Investissements d'Avenir" (ANR-11-IDEX-0007) operated by the French National Research Agency (ANR) for travel support for a stay at the Laboratoire de Tribologie et Dynamique des Systèmes (LTD). G.D.K. thanks the Fulbright Foundation for support of this work. We also thank Professors Bo Chen and Dmitri Makarov and Drs. Juliette Cayer-Barrioz, Denis Mazuyer, and Alejandro Boscoboinik for very useful discussions.

■ REFERENCES

(1) Beyer, M. K.; Clausen-Schaumann, H. Mechanochemistry: The Mechanical Activation of Covalent Bonds. *Chem. Rev.* **2005**, *105*, 2921−2948. Rosen, B. M.; Percec, V. Mechanochemistry: A reaction to stress. *Nature* **2007**, *446*, 381−382. Hickenboth, C. R.; Moore, J. S.; White, S. R.; Sottos, N. R.; Baudry, J.; Wilson, S. R. Biasing reaction pathways with mechanical force. *Nature* **2007**, *446*, 423−427. Craig, S. L. Mechanochemistry: A tour of force. *Nature* **2012**, *487*, 176−177.

(2) Duwez, A.-S.; Cuenot, S.; Jérôme, C.; Gabriel, S.; Jérôme, R.; Rapino, S.; Zerbetto, F. Mechanochemistry: targeted delivery of single molecules. *Nat. Nano.* **2006**, *1*, 122−125. Liang, J.; Fernandez, J. M. Mechanochemistry: One Bond at a Time. *ACS Nano* **2009**, *3*, 1628−1645. Ribas-Arino, J.; Shiga, M.; Marx, D. Understanding Covalent Mechanochemistry. *Angew. Chem., Int. Ed.* **2009**, *48*, 4190−4193.

(3) Beyer, M. K. The mechanical strength of a covalent bond calculated by density functional theory. *J. Chem. Phys.* **2000**, *112*, 7307−7312.

(4) Klein, I. M.; Husic, C. C.; Kovács, D. P.; Choquette, N. J.; Robb, M. J. Validation of the CoGEF Method as a Predictive Tool for Polymer Mechanochemistry. *J. Am. Chem. Soc.* **2020**, *142*, 16364−16381.

(5) Ong, M. T.; Leiding, J.; Tao, H.; Virshup, A. M.; Martínez, T. J. First Principles Dynamics and Minimum Energy Pathways for Mechanochemical Ring Opening of Cyclobutene. *J. Chem. Phys.* **2009**, *131*, 6377−6379.

(6) Subramanian, G.; Mathew, N.; Leiding, J. A generalized force-modified potential energy surface for mechanochemical simulations. *J. Chem. Phys.* **2015**, *143*, 134109.

(7) Wolinski, K.; Baker, J. Theoretical predictions of enforced structural changes in molecules. *Mol. Phys.* **2009**, *107*, 2403−2417.

(8) Makarov, D. E. Perspective: Mechanochemistry of biological and synthetic molecules. *J. Chem. Phys.* **2016**, *144*, No. 030901.

(9) Bell, G. Models for the specific adhesion of cells to cells. *Science* **1978**, *200*, 618−627.

(10) Evans, E.; Ritchie, K. Dynamic strength of molecular adhesion bonds. *Biophys. J.* **1997**, *72*, 1541−1555.

(11) Konda, S. S. M.; Brantley, J. N.; Bielawski, C. W.; Makarov, D. E. Chemical reactions modulated by mechanical stress: Extended Bell theory. *J. Chem. Phys.* **2011**, *135*, 164103−164108.

(12) Tysoe, W. On Stress-Induced Tribochemical Reaction Rates. *Tribol. Lett.* **2017**, *65*, 48.

(13) Spikes, H.; Tysoe, W. On the Commonality Between Theoretical Models for Fluid and Solid Friction, Wear and Tribochemistry. *Tribol. Lett.* **2015**, *59*, 1−14.

(14) Prandtl, L. Ein Gedankenmodell zur kinetischen Theorie der festen Körper. *Z. Angew. Math. Mech.* **1928**, *8*, 85. Furlong, O. J.; Manzi, S. J.; Pereyra, V. D.; Bustos, V.; Tysoe, W. T. Monte Carlo Simulations for Tomlinson Sliding Models for Non-Sinusoidal Periodic Potentials. *Tribol. Lett.* **2010**, *39*, 177−180. Article. Müser, M. Velocity dependence of kinetic friction in the Prandtl-Tomlinson model. *Phys. Rev. B* **2011**, *84*, No. 125419. Gnecco, E.; Roth, R.; Baratoff, A. Analytical expressions for the kinetic friction in the Prandtl-Tomlinson model. *Phys. Rev. B* **2012**, *86*, No. 035443. Manzi, S.; Tysoe, W.; Furlong, O. Temperature Dependences in the Tomlinson/Prandtl Model for Atomic Sliding Friction. *Tribol. Lett.* **2014**, *55*, 363−369.

(15) Eyring, H. Viscosity, Plasticity, and Diffusion as Examples of Absolute Reaction Rates. *J. Chem. Phys* **1936**, *4*, 283−291. Kauzmann, W.; Eyring, H. The Viscous Flow of Large Molecules. *J. Am. Chem. Soc.* **1940**, *62*, 3113−3125.

(16) Stauch, T.; Dreuw, A. Advances in Quantum Mechanochemistry: Electronic Structure Methods and Force Analysis. *Chem. Rev.* **2016**, *116*, 14137−14180. Ribas-Arino, J.; Marx, D. Covalent Mechanochemistry: Theoretical Concepts and Computational Tools with Applications to Molecular Nanomechanics. *Chem. Rev.* **2012**, *112*, 5412−5487.

(17) Asano, T.; Le Noble, W. J. Activation and reaction volumes in solution. *Chem. Rev.* **1978**, *78*, 407−489. Drljaca, A.; Hubbard, C. D.; van Eldik, R.; Asano, T.; Basilevsky, M. V.; le Noble, W. J. Activation and Reaction Volumes in Solution. 3. *Chem. Rev.* **1998**, *98*, 2167−2290. Röntgen, W. C. Kurze Mittheilung von Versuchen über den Einfluss des Druckes auf einige physikalische Erscheinungen. *Ann. Phys.* **1892**, *281*, 98−107.

(18) Cravotto, G.; Gaudino, E. C.; Cintas, P. On the mechanochemical activation by ultrasound. *Chem. Soc. Rev.* **2013**, *42*, 7521−7534.

(19) Brantley, J. N.; Konda, S. S. M.; Makarov, D. E.; Bielawski, C. W. Regiochemical Effects on Molecular Stability: A Mechanochemical Evaluation of 1,4- and 1,5-Disubstituted Triazoles. *J. Am. Chem. Soc.* **2012**, *134*, 9882−9885. Brantley, J. N.; Wiggins, K. M.; Bielawski, C. W. Unclicking the Click: Mechanically Facilitated 1,3-Dipolar Cycloreversions. *Science* **2011**, *333*, 1606−1609.
(20) Evans, M. G.; Polanyi, M. Some applications of the transition state method to the calculation of reaction velocities, especially in solution. *Trans. Farad. Soc.* **1935**, *31*, 875−894.
(21) Stearn, A. E.; Eyring, H. Pressure and Rate Processes. *Chem. Rev.* **1941**, *29*, 509−523.
(22) Jha, S. K.; Brown, K.; Todde, G.; Subramanian, G. A mechanochemical study of the effects of compression on a Diels-Alder reaction. *J. Chem. Phys* **2016**, *145*, No. 074307. Chen, B.; Hoffmann, R.; Cammi, R. The Effect of Pressure on Organic Reactions in Fluids—a New Theoretical Perspective. *Angew. Chem. Int. Ed* **2017**, *56*, 11126−11142.
(23) Suryanarayana, C. Mechanical alloying and milling. *Prog. Mater. Sci.* **2001**, *46*, 1−184. Rodríguez, B.; Bruckmann, A.; Rantanen, T.; Bolm, C. Solvent-Free Carbon-Carbon Bond Formations in Ball Mills. *Adv. Synth. Catal.* **2007**, *349*, 2213−2233. Sepelak, V.; Begin-Colin, S.; Le Caer, G. Transformations in oxides induced by high-energy ball-milling. *Dalton Trans.* **2012**, *41*, 11927−11948. Sohma, J. Mechanochemistry of polymers. *Prog. Polym. Sci.* **1989**, *14*, 451−596. Boldyrev, V. V.; Tkáčová, K. Mechanochemistry of Solids: Past, Present, and Prospects. *J. Mater. Syn. Process.* **2000**, *8*, 121−132. Levitas, V. I. High-pressure mechanochemistry: Conceptual multiscale theory and interpretation of experiments. *Phys. Rev.B* **2004**, *70*, No. 184118. Kipp, S.; Šepelák, V.; Becker, K. D. Mechanochemie: Chemie mit dem Hammer. *Chem. Unserer Zeit* **2005**, *39*, 384−392. Todres, Z. V. *Organic mechanochemistry and its practical applications*; Taylor&Francis, 2006. Varma, R. S. "Greener" chemical syntheses using mechanochemical mixing or microwave and ultrasound irradiation. *Green Chem. Lett. Rev.* **2007**, *1*, 37−45. (j) Mitchenko, S. A. Mechanochemistry in heterogeneous catalysis. *Theor. Exp. Chem.* **2007**, *43*, 211−228. Hick, S. M.; Griebel, C.; Restrepo, D. T.; Truitt, J. H.; Buker, E. J.; Bylda, C.; Blair, R. G. Mechanocatalysis for biomass-derived chemicals and fuels. *Green Chem.* **2010**, *12*, 468−474. Kucharski, T. J.; Boulatov, R. The physical chemistry of mechanoresponsive polymers. *J. Mater. Chem.* **2011**, *21*, 8237−8255. Do, J.-L.; Friščić, T. Mechanochemistry: A Force of Synthesis. *ACS Cent. Sci.* **2017**, *3*, 13−19. (n) Tan, D.; García, F. Main group mechanochemistry: from curiosity to established protocols. *Chem. Soc. Rev.* **2019**, *48*, 2274−2292.
(24) Piras, C. C.; Fernández-Prieto, S.; De Borggraeve, W. M. Ball milling: a green technology for the preparation and functionalisation of nanocellulose derivatives. *Nanoscale Adv.* **2019**, *1*, 937−947. James, S. L.; Adams, C. J.; Bolm, C.; Braga, D.; Collier, P.; Friscic, T.; Grepioni, F.; Harris, K. D. M.; Hyett, G.; Jones, W.; et al. Mechanochemistry: opportunities for new and cleaner synthesis. *Chem. Soc. Rev* **2012**, *41*, 413−447.
(25) Zhang, J.; Spikes, H. On the Mechanism of ZDDP Antiwear Film Formation. *Tribol. Lett.* **2016**, *63*, 1−15. Gosvami, N. N.; Bares, J. A.; Mangolini, F.; Konicek, A. R.; Yablon, D. G.; Carpick, R. W. Mechanisms of antiwear tribofilm growth revealed in situ by single-asperity sliding contacts. *Science* **2015**, *348*, 102−106. Felts, J. R.; Oyer, A. J.; Hernández, S. C.; Whitener, K. E., Jr.; Robinson, J. T.; Walton, S. G.; Sheehan, P. E. Direct mechanochemical cleavage of functional groups from graphene. *Nat. Commun.* **2015**, *6*, 6467.
(26) Boscoboinik, A.; Olson, D.; Adams, H.; Hopper, N.; Tysoe, W. T. Measuring and modelling mechanochemical reaction kinetics. *Chem. Commun.* **2020**, *56*, 7730−7733.
(27) Müser, M. H.; Dapp, W. B.; Bugnicourt, R.; Sainsot, P.; Lesaffre, N.; Lubrecht, T. A.; Persson, B. N. J.; Harris, K.; Bennett, A.; Schulze, K.; Rohde, S.; Ifju, P.; Sawyer, W. G.; Angelini, T.; Ashtari Esfahani, H.; Kadkhodaei, M.; Akbarzadeh, S.; Wu, J. J.; Vorlaufer, G.; Vernes, A.; Solhjoo, S.; Vakis, A. I.; Jackson, R. L.; Xu, Y.; Streator, J.; Rostami, A.; Dini, D.; Medina, S.; Carbone, G.; Bottiglione, F.; Afferrante, L.; Monti, J.; Pastewka, L.; Robbins, M. O.; Greenwood, J. A. Meeting the Contact-Mechanics Challenge. *Tribol. Lett.* **2017**, *65*, 118.
(28) Seema, P.; Behler, J.; Marx, D. Peeling by Nanomechanical Forces: A Route to Selective Creation of Surface Structures. *Phys. Rev.Lett.* **2015**, *115*, No. 036102. Seema, P.; Behler, J.; Marx, D. Force-induced mechanical response of molecule-metal interfaces: molecular nanomechanics of propanethiolate self-assembled monolayers on Au(111). *Phys. Chem. Chem. Phys.* **2013**, *15*, 16001−16011. Krüger, D.; Rousseau, R.; Fuchs, H.; Marx, D. Towards "Mechanochemistry:" Mechanically Induced Isomerizations of Thiolate−Gold Clusters. *Angew. Chem., Int. Ed.* **2003**, *42*, 2251−2253. Konôpka, M.; Rousseau, R.; Štich, I.; Marx, D. Detaching Thiolates from Copper and Gold Clusters: Which Bonds to Break? *J. Am. Chem. Soc.* **2004**, *126*, 12103−12111. Konôpka, M.; Turansky, R.; Dubecký, M.; Marx, D.; Štich, I. Molecular Mechanochemistry Understood at the Nanoscale: Thiolate Interfaces and Junctions with Copper Surfaces and Clusters. *J. Phys. Chem. C* **2009**, *113*, 8878−8887.
(29) Furlong, O. J.; Miller, B. P.; Tysoe, W. T. Shear-Induced Surface-to-Bulk Transport at Room Temperature in a Sliding Metal-Metal Interface. *Tribol. Lett.* **2011**, *41*, 257−261. Adams, H.; Miller, B. P.; Furlong, O. J.; Fantauzzi, M.; Navarra, G.; Rossi, A.; Xu, Y.; Kotvis, P. V.; Tysoe, W. T. Modeling Mechanochemical Reaction Mechanisms. *ACS Appl. Mater. Interfaces* **2017**, *9*, 26531−26538.
(30) Furlong, O.; Miller, B.; Tysoe, W. T. Shear-induced boundary film formation from dialkyl sulfides on copper. *Wear* **2012**, *274-275*, 183−187.
(31) Adams, H. L.; Garvey, M. T.; Ramasamy, U. S.; Ye, Z.; Martini, A.; Tysoe, W. T. Shear-Induced Mechanochemistry: Pushing Molecules Around. *J. Phys. Chem. C* **2015**, *119*, 7115−7123.
(32) Miller, B.; Furlong, O.; Tysoe, W. T. The Kinetics of Shear-Induced Boundary Film Formation from Dimethyl Disulfide on Copper. *Tribol. Lett.* **2013**, *49*, 39−46.
(33) Furlong, O.; Miller, B.; Tysoe, W. Shear-Induced Surface-to-Bulk Transport at Room Temperature in a Sliding Metal−Metal Interface. *Tribol. Lett.* **2011**, *41*, 257−261. Adams, H.; Miller, B. P.; Kotvis, P. V.; Furlong, O. J.; Martini, A.; Tysoe, W. T. In Situ Measurements of Boundary Film Formation Pathways and Kinetics: Dimethyl and Diethyl Disulfide on Copper. *Tribol. Lett.* **2016**, *62*, 1−9.
(34) Rana, R.; Long, D.; Kotula, P.; Xu, Y.; Olson, D.; Galipaud, J.; LeMogne, T.; Tysoe, W. T. Insights into the Mechanism of the Mechanochemical Formation of Metastable Phases. *ACS Appl. Mater. Interfaces* **2021**, *13*, 6785−6794.
(35) Luan, B.; Robbins, M. O. The breakdown of continuum models for mechanical contacts. *Nature* **2005**, *435*, 929−932.
(36) Bailey, A.; Mosey, N. J. Prediction of reaction barriers and force-induced instabilities under mechanochemical conditions with an approximate model: A case study of the ring opening of 1,3-cyclohexadiene. *J. Chem. Phys.* **2012**, *136*, No. 044102. Dudko, O.; Hummer, G.; Szabo, A. Intrinsic Rates and Activation Free Energies from Single-Molecule Pulling Experiments. *Phys. Rev. Lett.* **2006**, *96*, No. 108101. Avdoshenko, S. M.; Makarov, D. E. Reaction Coordinates and Pathways of Mechanochemical Transformations. *J. Phys. Chem. B* **2016**, *120*, 1537−1545. Quapp, W.; Bofill, J. M.; Ribas-Ariño, J. Analysis of the Acting Forces in a Theory of Catalysis and Mechanochemistry. *J. Phys. Chem. A* **2017**, *121*, 2820−2838. Quapp, W.; Bofill, J. M. Mechanochemistry on the Müller−Brown surface by Newton trajectories. *Int. J. Quantum Chem.* **2018**, *118*, No. e25522.
(37) Rana, R.; Bavisotto, R.; Hopper, N.; Tysoe, W. T. Inducing High-Energy-Barrier Tribochemical Reaction Pathways; Acetic Acid Decomposition on Copper. *Tribol. Lett.* **2021**, *69*, 32.
(38) Henkelman, G.; Uberuaga, B. P.; Jonsson, H. A climbing image nudged elastic band method for finding saddle points and minimum energy paths. *J. Chem. Phys* **2000**, *113*, 9901−9904. Henkelman, G.; Jónsson, H. Improved tangent estimate in the nudged elastic band method for finding minimum energy paths and saddle points. *J. Chem. Phys* **2000**, *113*, 9978−9985. Sheppard, D.; Henkelman, G. Paths to which the nudged elastic band converges. *J. Comput. Chem.* **2011**, *32*, 1769−1771.

https://doi.org/10.1021/acs.jpcc.2c03033
J. Phys. Chem. C 2022, 126, 11585−11593

(39) Miller, W. H.; Handy, N. C.; Adams, J. E. Reaction path Hamiltonian for polyatomic molecules. *J. Chem. Phys.* **1980**, *72*, 99−112. Kraka, E. Reaction Path Hamiltonian and its Use for Investigating Reaction Mechanisms. In *Encyclopedia of Computational Chemistry*; Wiley 1998.
(40) Dienwiebel, M.; Verhoeven, G. S.; Pradeep, N.; Frenken, J. W. M.; Heimberg, J. A.; Zandbergen, H. W. Superlubricity of Graphite. *Phys. Rev. Lett.* **2004**, *92*, No. 126101.
(41) Barth, J. V.; Brune, H.; Ertl, G.; Behm, R. J. Scanning Tunneling Microscopy Observations on the Reconstructed Au(111) Surface - Atomic-Structure, Long-Range Superstructure, Rotational Domains, and Surface-Defects. *Phys. Rev. B* **1990**, *42*, 9307−9318.
(42) Rana, R.; Bavisotto, R.; Hou, K.; Tysoe, W. T. Surface Chemistry at the Solid-Solid Interface: Mechanically Induced Reaction Pathways of C_8 Carboxylic Acid Monolayers on Copper. *Phys. Chem. Chem. Phys.* **2021**, *23*, 17803−17812.
(43) Furlong, O. J.; Miller, B. P.; Li, Z.; Walker, J.; Burkholder, L.; Tysoe, W. T. The Surface Chemistry of Dimethyl Disulfide on Copper. *Langmuir* **2010**, *26*, 16375−16380.
(44) Meyer, E.; Hug, H. J.; Bennewitz, R. *Scanning probe microscopy : the lab on a tip*; Springer, 2011.
(45) Cook, S. M.; Lang, K. M.; Chynoweth, K. M.; Wigton, M.; Simmonds, R. W.; Schäffer, T. E. Practical implementation of dynamic methods for measuring atomic force microscope cantilever spring constants. *Nanotechnology* **2006**, *17*, 2135−2145.
(46) Furlong, O. J.; Miller, B. P.; Kotvis, P.; Tysoe, W. T. Low-Temperature, Shear-Induced Tribofilm Formation from Dimethyl Disulfide on Copper. *ACS Appl. Mater. Interfaces* **2011**, *3*, 795−800.
(47) Remoissenet, M.; Peyrard, M. A new simple model of a kink bearing Hamiltonian. *J. Phys. C: Solid State Phys.* **1981**, *14*, L481.

https://doi.org/10.1021/acs.jpcc.2c03033
J. Phys. Chem. C 2022, 126, 11585−11593